Generalized Schamel nonlinear Schrödinger dynamics of ion-acoustic wave packets in electronegative plasmas with trapped negative ions

Chérif Souleman Panguetna [1,*] Conrad Bertrand Tabi [2,†] Stéphanie Ganyou [1,‡] and Timoléon Crépin Kofané [1,2,§]
[1]*Laboratory of Mechanics, Materials and Structures, Department of Physics, Faculty of Science, University of Yaoundé I, Yaoundé, Cameroon*
[2]*Department of Physics and Astronomy, Botswana International University of Science and Technology, Palapye, Botswana*

(Received 30 June 2026; revised 9 September 2026; accepted 7 October 2026; published 28 October 2026)

We investigate the amplitude modulation of ion-acoustic wave packets in an unmagnetized electronegative plasma composed of cold positive ions, Boltzmann electrons, and negative ions following a Schamel trapped-particle distribution. The trapped-particle description is relevant to weakly collisional electronegative plasmas supporting Bernstein–Greene–Kruskal (BGK)-type potential structures and ion-hole equilibria, where a fraction of the negative-ion population can become trapped in the self-consistent wave potential. Unlike conventional analytic closures (Boltzmann, Tsallis, κ-distributed, nonthermal), which we show can only produce a cubic envelope nonlinearity regardless of their parametrization, this nonanalytic trapped-particle response naturally yields a generalized Schamel nonlinear Schrödinger equation combining the familiar cubic term with a genuinely noninteger $|\Psi|^{1/2}\Psi$ contribution. Derived through both a long-wavelength (Gardner-Schamel) limit and the full modulated-wave-packet limit, the resulting dispersion, cubic, and fractional coefficients are obtained in closed form. Two results stand out. First, the maximum modulational growth rate depends nonmonotonically on the negative-ion concentration, exhibiting an interior optimum that maximizes the instability above a critical temperature ratio, and, near the long-wavelength threshold, a finite concentration window outside of which the instability vanishes entirely. Second, a split-step Fourier analysis shows that the trapped-ion population breaks the time-symmetry of the Peregrine and Akhmediev rogue-wave solutions, causing them to build up faster than they decay, a signature invisible in the peak amplitude alone. These results extend previous electronegative plasma models and provide testable predictions for nonlinear wave localization in plasmas containing trapped particles.

DOI: 10.1103/9x1y-tnll

I. INTRODUCTION

Modulational instability (MI) is the generic mechanism by which a weakly nonlinear, slowly modulated wave train in a dispersive medium amplifies small perturbations of its envelope into large, localized excursions, rogue waves [1]. Its nonlinear outcome is conventionally described, for a wide class of dispersive systems, by the cubic nonlinear Schrödinger equation (NLSE) and its rational and periodic breather solutions (Peregrine [2], Akhmediev [3], Kuznetsov-Ma [4,5]). A comprehensive account of modulational interactions in plasmas, including coherent and broadband descriptions, can be found in the monograph of Vladimirov *et al*. [6]. In plasma physics, the amplitude modulation of ion-acoustic wave packets in electronegative plasmas (plasmas containing, in addition to electrons and positive ions, a population of negative ions) has been studied extensively through the reductive perturbation method, which reduces the governing fluid-Poisson system to an NLSE for the slowly varying wave envelope [7,8]. For the purely Boltzmann (analytic) closure, this includes an explicit MI and rogue-wave analysis [8–10]. In essentially all such treatments, the electron and negative-ion populations are described by an analytic equilibrium closure (Boltzmann, nonextensive Tsallis, κ-distributed, or nonthermal Cairns), and the resulting envelope equation is invariably cubic, $i\partial_\sigma\Psi + P\partial_\zeta^2\Psi + Q|\Psi|^2\Psi = 0$. The specific closure only reshapes the dispersion and nonlinearity coefficients P, Q; it never changes the order of the nonlinearity. This is not a coincidence specific to any one closure, but a structural consequence of the reductive perturbation method itself, as we show in Sec. II.

A genuinely fractional-order envelope nonlinearity, $|\Psi|^{2\sigma}\Psi$ with noninteger σ, therefore requires a mechanism that breaks the analyticity of the underlying equilibrium closure at the unperturbed state. A well-established such mechanism is the trapping of a fraction of a plasma species in the self-consistent potential of the wave itself [11]: the resulting equilibrium density acquires a nonanalytic $|\phi|^{3/2}\,\mathrm{sgn}(\phi)$ correction in addition to the usual Boltzmann terms, giving rise to the Schamel equation [a modified Korteweg–de Vries (KdV) equation with a $\sqrt{|\phi|}$ nonlinearity] in the long-wavelength limit, and to a fractional-order "Schamel-NLSE" for modulated wave packets [12]. Such trapped-particle structures, including electron and ion holes, Bernstein–Greene–Kruskal (BGK) modes [13], and the electrostatic

*Contact author: cherifps@yahoo.fr
†Contact author: tabic@biust.ac.bw
‡Contact author: stephanieganyou@gmail.com
§Contact author: kofanet@biust.ac.bw

Published by the American Physical Society under the terms of the Creative Commons Attribution 4.0 International license. Further distribution of this work must maintain attribution to the author(s) and the published article's title, journal citation, and DOI.

solitary waves recorded *in situ* by spacecraft such as GEOTAIL and FAST in the auroral zone, the magnetosphere, and the solar wind [14,15], are a well-documented feature of real, weakly collisional plasmas. The trapped-particle route to a fractional envelope nonlinearity is therefore not merely a mathematical curiosity but a physically motivated alternative to the conventional analytic closures. Directly relevant to the system studied here, Peregrine solitons have already been observed experimentally in a laboratory multicomponent plasma containing negative ions [16], providing direct experimental precedent for rogue-wave dynamics in electronegative plasmas, albeit for the standard cubic-NLS mechanism rather than the trapped-particle route considered in this paper.

Existing studies combining electron and ion trapping with electronegative plasmas have so far trapped the electron population, retaining a Boltzmann response for the negative ions, and have been restricted to the long-wavelength (KdV and Burgers-type) limit rather than the modulated wave-packet limit [17]. Conversely, existing Schamel-NLSE derivations for modulated wave packets [12,18] are formulated for different physical systems (electron-acoustic waves, degenerate quantum complex plasmas) and present the fractional term as the sole nonlinearity, suggesting that the standard analytic cubic contribution is not retained alongside it. The broader study of MI and rogue-wave dynamics in non-Maxwellian and trapped-particle plasmas remains an active area, with recent work extending these techniques to combined suprathermal-trapped electron distributions [19], to quantum dusty plasmas [20], and to magnetosonic wave packets supporting Akhmediev, Kuznetsov-Ma, and rogue-wave structures [21].

In this paper we extend the electronegative plasma model of [7], consisting of cold mobile positive ions, Boltzmann electrons, and Boltzmann negative ions, by replacing the negative-ion closure with a Schamel-type trapped or free distribution: trapping is applied to the negative-ion population itself, rather than to the electrons. Both the long-wavelength (Gardner-Schamel) limit and the full modulated-wave-packet limit are derived, and the latter is shown to be governed by a mixed cubic-and-fractional Schamel-NLS equation in which the standard analytic cascade (cubic term) and the trapped-particle contribution (fractional term) coexist self-consistently and reduce correctly to the known pure-cubic [7] and pure-fractional [12] limits. We further show that the long-wavelength and modulated-wave-packet limits of the same physical system require different distinguished orderings of the trapping deficiency parameter. Beyond the derivation itself, we characterize the resulting MI in closed form and identify a nonmonotonic dependence of the maximum growth rate on the negative-ion concentration, including regimes where trapping switches the instability on or off entirely. A split-step Fourier analysis further shows that the trapped-ion population breaks the time-symmetry of the Peregrine and Akhmediev rogue-wave solutions of the background cubic equation, causing them to build up faster than they decay.

The present analysis is restricted to the long-wavelength ion-acoustic regime $k\lambda_D \ll 1$; the short-wavelength limit $k\lambda_D \sim 1$, where ion oscillations acquire Langmuir-wave character and quasineutrality breaks down [22], falls outside the scope of the multiple-scales expansion employed here.

The remainder of this paper is organized as follows. Section II introduces the electronegative plasma model and discusses why a nonanalytic closure is required to obtain a fractional envelope equation. Section III presents the linear dispersion relation. Sections IV and V derive the Gardner-Schamel and Schamel-NLS equations, respectively. The MI analysis is reported in Sec. VI, followed by numerical simulations of rogue-wave dynamics in Sec. VII. The physical implications of the results are discussed in Sec. VIII before concluding remarks are given in Sec. IX.

II. GOVERNING EQUATIONS

We consider a one-dimensional, unmagnetized, collisionless electronegative plasma made of (i) cold, mobile, inertial positive ions; (ii) Boltzmann electrons; and (iii) negative ions following a Schamel-type trapped or free distribution. Lengths are normalized to the electron Debye length, time to the inverse ion plasma frequency, velocities to the ion-acoustic speed, and the electrostatic potential to T_e/e. The normalized continuity and momentum equations for the positive-ion fluid, closed by Poisson's equation, read

$$\partial_t n_p + \partial_x (n_p u_p) = 0, \tag{1}$$

$$\partial_t u_p + u_p\, \partial_x u_p = -\partial_x \phi, \tag{2}$$

$$\partial_x^2 \phi = n_e + n_n - n_p, \tag{3}$$

with the Boltzmann electron closure

$$n_e = (1-\alpha)\, e^{\phi}, \tag{4}$$

and the Schamel trapped or free closure for the negative ions

$$n_n = \alpha\big[\, 1 + \kappa\phi + \tfrac{1}{2}(\kappa\phi)^2 + \tfrac{1}{6}(\kappa\phi)^3 - c\,(1-\beta)\,(\kappa\phi)^{3/2} + \cdots \big], \tag{5}$$

with $c = 4/(3\sqrt{\pi}) = 0.7523\ldots$. Here $\alpha \equiv n_{n0}$ is the equilibrium negative-ion concentration ($n_{e0} = 1-\alpha$, $n_{p0} = 1$ by quasineutrality), $\kappa \equiv T_e/T_n$ is the electron-to-negative-ion temperature ratio, and $\beta \leqslant 1$ is the Schamel trapping parameter: $\beta = 1$ recovers the pure Boltzmann response of [7] (the fractional term vanishes identically), while $\beta < 1$ corresponds to a flat-topped (vortex-depleted) trapped population. More precisely, $\beta \in (-1, 1)$: for $0 < \beta < 1$ the trapped population is partially depleted relative to Boltzmann, while $\beta < 0$ describes a vortex-like distribution with a local maximum at zero velocity, characteristic of particles reflected at the wave potential barrier [11]. Throughout this work we consider $0 < 1-\beta \ll 1$, i.e., a small but nonzero departure from the Boltzmann response. Physically, a population of trapped negative ions with this distribution is expected whenever the negative-ion bounce frequency $\omega_{\text{bounce}} = (e\phi_0 k^2/m_n)^{1/2}$ exceeds the negative-ion collision frequency, a condition met in low-pressure electronegative discharges (SF_6, O_2, Cl_2), the *D*-region ionosphere, and cometary plasma environments, all of which are established contexts for Schamel-type trapped-particle models [11,13]. We define, for later use,

$$D \equiv (1-\alpha) + \alpha\kappa, \quad E \equiv (1-\alpha) + \alpha\kappa^2,$$
$$G \equiv (1-\alpha) + \alpha\kappa^3. \tag{6}$$

Suppose, for the moment, that the fractional term in Eq. (5) is absent, so that $n_n(\phi)$ is analytic. The reductive perturbation method expands all fields in powers of a formal small parameter ε and a fast-phase harmonic series, and extracts the envelope equation from the solvability (Fredholm) condition of the singular linear operator that recurs, order by order, at the fundamental harmonic. Because this operator, and hence its left null vector, is the same at every order, while the nonlinear feedback entering the relevant solvability condition is generated by a finite cascade of harmonic products (the second and zeroth harmonics, themselves quadratic in the fundamental), any analytic closure necessarily produces a feedback term of cubic order in the envelope amplitude at leading order, regardless of the closure's specific functional form. The closure only enters through the numerical values of the coefficients D, E, G (and the analogous coefficients of higher Taylor terms, which do not contribute at leading order); it cannot alter the order $\sigma = 1$ of the nonlinearity. The present derivation indicates that, within the reductive perturbation framework considered here and for closures that are analytic at $\phi = 0$, this conclusion applies equally to Boltzmann, Tsallis, κ, and Cairns closures, and is consistent with published nonextensive electron-acoustic NLSE derivations of this type [23]. It does not exclude fractional envelope nonlinearities arising through other mechanisms (e.g., nonanalytic closures, fully kinetic treatments, or higher-order perturbation theory), and should be understood as a statement about the structure of the multiple-scales hierarchy rather than a general theorem of plasma kinetic theory.

A genuinely fractional power therefore requires a closure that is non-analytic at $\phi = 0$, which is precisely the effect of the trapped-particle term in Eq. (5).

III. LINEAR WAVE PROPERTIES

Linearizing Eqs. (1) to (3) about the equilibrium with $n_{p1}, u_{p1}, \phi_1 \propto \exp[\mathrm{i}(kx - \omega t)]$ gives $n_{p1} = k^2\phi_1/\omega^2$, $u_{p1} = (k/\omega)\phi_1$, and the dispersion relation

$$\omega^2 = \frac{k^2}{D + k^2}. \tag{7}$$

The long-wavelength ($k \to 0$) ion-acoustic speed of the composite system is $V_0 = 1/\sqrt{D}$, and the group velocity is $V_g(k) = \mathrm{d}\omega/\mathrm{d}k = D/(D + k^2)^{3/2}$.

IV. LONG-WAVELENGTH LIMIT: THE GARDNER-SCHAMEL EQUATION

A single, slowly varying solitary disturbance is considered first (no fast carrier), using the Gardner-Morikawa stretching [24] $\xi = \sqrt{\varepsilon}\,(x - V_0 t)$, $\tau = \varepsilon^{3/2}t$, with $\phi = \varepsilon\phi_1 + \varepsilon^2\phi_2 + \cdots$ (similarly for n_p, u_p). For the trapped-particle term to balance the standard analytic nonlinearity at the same order, the trapping deficiency must scale as

$$1 - \beta = \sqrt{\varepsilon}\, b_1, \quad b_1 = O(1), \tag{8}$$

since $\phi^{3/2} \sim \varepsilon^{3/2}$ and $(1 - \beta)\phi^{3/2} \sim \varepsilon^2$ matches the order of the quadratic Taylor nonlinearity. Carrying out the standard elimination of the second-order fields n_{p2}, u_{p2}, ϕ_2 (which cancel identically once the dispersion relation $D = 1/V_0^2$ is imposed) yields the closed evolution equation

$$\partial_\tau\phi_1 + \tilde{A}\,\phi_1\partial_\xi\phi_1 + \tilde{C}\,\sqrt{\phi_1}\,\partial_\xi\phi_1 + \tilde{B}\,\partial_\xi^3\phi_1 = 0, \tag{9}$$

with

$$\tilde{A} = \frac{EV_0^3}{2} - \frac{3}{2V_0}, \quad \tilde{C} = -\frac{3}{4}FV_0^3,$$
$$\tilde{B} = -\frac{V_0^3}{2}, \quad F \equiv \alpha\, c\, b_1\, \kappa^{3/2}. \tag{10}$$

As $\alpha \to 0$ (no negative ions), $D = E = V_0 = 1$ and $F = 0$, so that $\tilde{A} = -1$, $\tilde{B} = -1/2$: Eq. (9) reduces exactly to the standard ion-acoustic KdV equation, providing a check on the derivation. Equation (9) is itself a new Gardner-Schamel equation for an electronegative plasma with trapped negative ions, reducing to the known electronegative Gardner equation as $\beta \to 1$.

An interesting feature of this asymptotic ordering is that the trapped-particle contribution, Eq. (8), enters at exactly the same order as the conventional quadratic nonlinearity. This balance is a direct consequence of the distinguished scaling adopted for the trapping parameter and, as we show next, does not carry over to the envelope problem, which requires a different ordering altogether.

V. MODULATED WAVE PACKETS: THE SCHAMEL-NLS EQUATION

A. Distinguished ordering for the envelope problem

For a modulated wave packet with finite carrier wave number k, the relevant balance is between the trapped-particle nonlinearity and the analytic cubic feedback term (rather than the dispersive term, as in Sec. IV), and this requires a different ordering of the trapping deficiency

$$1 - \beta = \varepsilon^{3/2}\, b_1 \quad \text{(envelope problem)}, \tag{11}$$

one power of $\sqrt{\varepsilon}$ smaller than in Eq. (8). With this ordering, $(1 - \beta)(\kappa\phi)^{3/2} \sim \varepsilon^3$, matching the order of the standard cubic feedback term in the fundamental-harmonic compatibility condition derived below.

The consistency of this distinguished limit may be verified explicitly. In the multiple-scales hierarchy, the fundamental-harmonic solvability condition arises at order ε^3. The cubic nonlinearity $Q_c|\Psi|^2\Psi$ appears because the second-harmonic and mean-flow corrections, generated at $O(\varepsilon^2)$, feed back into the $O(\varepsilon^3)$ equation through products of the form $|\Psi|^2\Psi \sim \varepsilon^3$. The Schamel trapped-particle correction to the negative-ion density contains a term proportional to $(1 - \beta)(\kappa\phi)^{3/2}$; with the ordering (11), this scales as $\varepsilon^{3/2} \cdot \varepsilon^{3/2} = \varepsilon^3$, the same order as the cubic feedback. This coincidence is unique: a weaker ordering such as $(1 - \beta) \sim \varepsilon$ would place the fractional term at $O(\varepsilon^{5/2})$, making it dominant and suppressing the cubic contribution, while a stronger ordering $(1 - \beta) \sim \varepsilon^2$ would render it subleading at $O(\varepsilon^{7/2})$. The choice (11) is therefore the unique distinguished limit that produces the mixed cubic-and-fractional equation obtained below, with both contributions entering the solvability condition at the same order.

B. Multiple-scales expansion

Using the stretched coordinates $\zeta = \varepsilon(x - V_g t)$, $\sigma = \varepsilon^2 t$, each field is expanded in harmonics of the fast phase $\theta = kx - \omega t$,

$$n_p = 1 + \sum_{n\geqslant 1} \varepsilon^n \sum_l n_l^{(n)}(\zeta, \sigma)\, e^{il\theta} \tag{12}$$

(similarly for u_p, ϕ), with the reality condition $A_{-l}^{(n)} = (A_l^{(n)})^*$. Substituting into Eqs. (1)–(3) and collecting terms order by order in ε and harmonic by harmonic yields, at $O(\varepsilon)$, $l = 1$, the linear relations of Sec. III.

At $O(\varepsilon^2)$, $l = 2$, the three field equations close algebraically:

$$\phi_2 = \frac{(3k^4 - E\omega^4)\,\phi_1^2}{2\omega^2(D\omega^2 + 4k^2\omega^2 - k^2)}, \tag{13}$$

with n_2, u_2 given by analogous rational expressions in k, ω, D, E.

At $O(\varepsilon^2)$, $l = 0$, the continuity and momentum equations are satisfied trivially since their advective nonlinear terms cancel exactly between the counterpropagating $\pm k$ contributions of the fundamental harmonic; only Poisson's equation is nontrivial, giving $n_0 = D\phi_0 + E\phi_1\phi_1^*$. The values of ϕ_0, u_0 themselves follow from the well-known long-wave or short-wave resonance mechanism, obtained by integrating the $O(\varepsilon^3)$, $l = 0$ continuity and momentum equations once (for bounded, localized solutions)

$$\begin{aligned} n_0 &= D\phi_0 + E\phi_1\phi_1^*, \\ u_0 &= V_g n_0 - (n_1 u_1^* + n_1^* u_1), \\ \phi_0 &= V_g u_0 - u_1 u_1^*, \end{aligned} \tag{14}$$

whose solution is proportional to $\phi_1\phi_1^*$ with a common resonance denominator $DV_g^2 - 1$, vanishing precisely at the expected long-wave resonance $V_g = V_0$ [25].

At $O(\varepsilon^2)$, $l = 1$, the homogeneous linear operator recurs, and the solvability condition for the second-order corrections (n_1', u_1', ϕ_1') to the fundamental harmonic gives the group velocity, $V_g = \mathrm{d}\omega/\mathrm{d}k$, while the particular solution is

$$\begin{aligned} \phi_1' &= \frac{\mathrm{i}(2k^2 - D)}{k(D + k^2)}\,\partial_\zeta \phi_1, \\ n_1' &= -\frac{\mathrm{i}D}{k}\,\partial_\zeta \phi_1, \\ u_1' &= \frac{\mathrm{i}(k^2 - D)}{k\sqrt{D + k^2}}\,\partial_\zeta \phi_1. \end{aligned} \tag{15}$$

At $O(\varepsilon^3)$, $l = 1$, the continuity, momentum and Poisson equations admit a solution for the next-order corrections (n_1'', u_1'', ϕ_1'') if and only if the forcing [built from Eqs. (13) to (15) and the trapped-particle term] is orthogonal to the left null vector $v = (-\mathrm{i}/\omega, -\mathrm{i}k/\omega^2, 1)$ of the recurring singular operator. This solvability condition is the sought Schamel-NLS equation

$$\mathrm{i}\,\partial_\sigma \Psi + P\,\partial_\zeta^2 \Psi + Q_c\,|\Psi|^2\Psi + Q_f\,|\Psi|^{1/2}\Psi = 0, \tag{16}$$

where $\Psi \equiv \phi_1^{(1)}$. Equation (16) preserves the standard dispersive structure of the classical cubic NLS while introducing an additional nonlinear mechanism associated with trapped particles; the coexistence of both contributions, rather than the fractional term replacing the cubic one, distinguishes the present result from previously reported Schamel-NLS equations [12,18]. Physically, the cubic term reflects the collective fluid response of the plasma, whereas the fractional contribution originates from particles trapped inside the wave potential; the resulting dynamics therefore combines macroscopic fluid effects with kinetic trapping within a single envelope equation.

The dispersion coefficient is found to be

$$P = -\frac{3Dk}{2(D + k^2)^{5/2}}, \tag{17}$$

which coincides identically with the structural identity $P = \frac{1}{2}\,\mathrm{d}^2\omega/\mathrm{d}k^2$, for all D, as it must since P is fixed by the linear dispersion relation alone, independently of the nonlinear closure. At $D = 1$ ($\alpha = 0$), Eq. (17) also reproduces the parallel-modulation ($\theta = 0$) ion-acoustic result of [25].

The cubic coefficient, obtained from the analytic part of the cascade above, is

$$Q_c = \frac{\left[\begin{aligned} &27D^6 + 90D^5k^2 - 18D^4E + 105D^4k^4 \\ &- 66D^3Ek^2 + 45D^3k^6 + 3D^2E^2 - 84D^2Ek^4 \\ &+ 9D^2Gk^2 - 3DE^2k^2 - 42DEk^6 + 9DGk^4 \\ &- 3Dk^{10} - E^2k^4 - 6Ek^8 + 3Gk^6 \end{aligned}\right]}{12k(D + k^2)^{3/2}(3D^2 + 3Dk^2 + k^4)}. \tag{18}$$

In the long-wavelength limit, at $\alpha = 0$ ($D = E = G = 1$), this gives $Q_c \to 1/(3k)$, in agreement with the corresponding limit quoted by the authors of [25].

The fractional coefficient Q_f arises from the direct contribution of the trapped-particle term to the $O(\varepsilon^3)$ Poisson equation, through the fundamental Fourier content of the (even, density-type) regularized function $\phi|\phi|^{1/2}$. Writing $\phi = 2\varepsilon|\Psi|\cos(\theta + \chi)$, one finds $\cos u\,|\cos u|^{1/2} = g^*\cos u + (\text{odd harmonics} \geqslant 3)$, with

$$g^* = \frac{4}{\pi}\int_0^{\pi/2} \cos^{5/2}\theta\,\mathrm{d}\theta = \frac{2}{\pi}B\left(\frac{1}{2}, \frac{7}{4}\right) = 0.915312\ldots, \tag{19}$$

giving

$$Q_f = -\frac{\sqrt{2}\,g^*\,\alpha\,b_1\,c\,\kappa^{3/2}\,\omega^3}{2k^2}, \quad c = \frac{4}{3\sqrt{\pi}} = 0.752253\ldots, \tag{20}$$

which vanishes, as required, in the limits $\alpha \to 0$ (no negative ions) and $b_1 \to 0$ (pure Boltzmann response, $\beta \to 1$).

The exponent of the fractional term is not a free fitting parameter: it is fixed at $\sigma = 1/4$ in the convention $|\Psi|^{2\sigma}\Psi$ by the trapped-particle mechanism itself (Sec. V B), and this value has two direct structural consequences. First, single-soliton envelope solutions of the pure-σ equation scale as $\mathrm{sech}^{1/\sigma}$; the Schamel value $\sigma = 1/4$ therefore predicts a markedly wider, flatter envelope profile than the familiar sech^2 shape of the cubic ($\sigma = 1$) limit, at the same background amplitude; in principle a directly observable signature of trapping. Second, $\sigma = 1/4$ is far below the one-dimensional L^2-critical value

$\sigma = 2$ at which finite-time collapse becomes possible: the trapped-particle contribution can never destabilize the envelope solitons of this system in the way a sufficiently strong higher-order nonlinearity could.

VI. MODULATIONAL STABILITY

Throughout this section we use the shorthand $D \equiv (1-\alpha)+\alpha\kappa$, $E \equiv (1-\alpha)+\alpha\kappa^2$, $G \equiv (1-\alpha)+\alpha\kappa^3$ [Eq. (6)], where α is the negative-ion concentration, $\kappa = T_e/T_n$ the temperature ratio, and b_1 the trapping-deficiency amplitude; P, Q_c, and Q_f are as given in Eqs. (17), (18), and (20). As is standard in the NLS framework, the modulational instability threshold K_c is derived here for a quasimonochromatic (narrow-band) wave packet. The broad-spectrum regime, in which spectral-width effects modify the threshold condition [26], constitutes a distinct problem not considered here.

For a uniform background $\Psi = \Psi_0 \exp[\mathrm{i}(Q_c|\Psi_0|^2 + Q_f|\Psi_0|^{1/2})\sigma]$, the standard linear stability analysis of Eq. (16) against long-wavelength perturbations $\propto \exp[\mathrm{i}(K\zeta - \Omega\sigma)]$ gives the generalized dispersion relation

$$\Omega^2 = P^2K^2\big[K^2 - K_c^2\big],$$
$$K_c^2 = \frac{2}{P}\big(Q_c|\Psi_0|^2 + \tfrac{1}{4}Q_f|\Psi_0|^{1/2}\big), \tag{21}$$

which reduces to the familiar cubic-NLS criterion when $Q_f = 0$ ($K_c = \sqrt{2Q_c|\Psi_0|^2/P}$) and to the pure fractional-NLS result $K_c = \sqrt{Q_f|\Psi_0|^{1/2}/(2P)}$ when $Q_c = 0$. The stability criterion thus retains the familiar structure of the cubic NLS while being modified by the additional fractional contribution: trapped particles influence not only the value of the instability threshold but also the full range of unstable perturbation wavenumbers. The wave is modulationally unstable for $K < K_c$ whenever $P(Q_c|\Psi_0|^2 + \frac{1}{4}Q_f|\Psi_0|^{1/2}) > 0$, leading to bright envelope solitons in that regime, and is stable (dark or gray solitons) otherwise. Because $Q_f \propto \alpha\, b_1$, the trapped negative-ion population shifts the instability threshold K_c and can, for sufficiently large trapping deficiency b_1, change the sign of the bracket in Eq. (21) at fixed P, Q_c, i.e., trapping can qualitatively change the stability profile obtained from the purely analytic (Boltzmann) closure of [7].

Figure 1 illustrates the wave-number dependence of P, Q_c, Q_f and the modulational threshold K_c for $\kappa = 2$ and several values of the negative-ion concentration α [Figs. 1(c) and 1(d) additionally fix the trapping-deficiency amplitude $b_1 = 1$ and, for Fig. 1(d), $|\Psi_0| = 0.3$]. The dispersion coefficient $P(k)$ [Fig. 1(a)] is negative throughout and attains a minimum near $k \simeq 0.5$; increasing α deepens this minimum but leaves the small- and large-k behavior essentially unchanged since P depends on the closure only through the linear coefficient D. The cubic coefficient $Q_c(k)$ [Fig. 1(b)] changes sign near $k \simeq 1.5-2$, the usual zerononlinearity point of ion-acoustic NLS theory, shifted by α; modulational stability is therefore already nonmonotonic in k before any trapping is introduced. The fractional coefficient $Q_f(k)$ [Fig. 1(c)] is negative throughout the displayed range and grows markedly in magnitude with α, reflecting the direct proportionality $Q_f \propto \alpha$. Figure 1(d) shows the resulting threshold $K_c(k)$: for the chosen background amplitude, the bracket in Eq. (21) is negative (no MI)

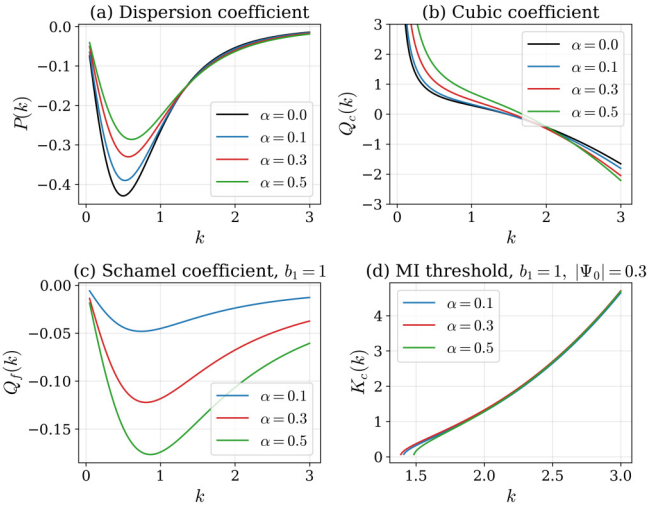


FIG. 1. Wave-number dependence of (a) the dispersion coefficient P, (b) the cubic coefficient Q_c, (c) the fractional (Schamel) coefficient Q_f, and (d) the modulational instability threshold K_c, for $\kappa = 2$ and several values of the negative-ion concentration α. Panels (c) and (d) use $b_1 = 1$; panel (d) additionally uses $|\Psi_0| = 0.3$ and is only plotted where $K_c^2 > 0$.

for k below approximately 1.4, where $Q_c > 0$ but $P < 0$, and instability only sets in beyond that point once the sign of Q_c has reversed; larger α shifts this threshold slightly toward smaller k. The qualitative trend is robust to the precise value of b_1, which mainly rescales the magnitude of the Q_f contribution without altering the sign structure shown here.

A. Growth rate

Beyond the threshold K_c, the full instability growth rate follows directly from the same linearization. Writing $\Psi = [\Psi_0 + \psi(\zeta,\sigma)]\, e^{\mathrm{i}\Theta\sigma}$, with $\Theta = Q_c|\Psi_0|^2 + Q_f|\Psi_0|^{1/2}$ and seeking sideband perturbations $\psi \propto e^{\mathrm{i}(K\zeta - \Omega\sigma)}$, the same generalized dispersion relation $\Omega^2 = P^2K^2(K^2 - K_c^2)$ of Eq. (21) applies. For $0 \leqslant K < K_c$, Ω is purely imaginary, $\Omega = \mathrm{i}\Gamma$, and the perturbation grows as $e^{\Gamma\sigma}$ with

$$\Gamma(K) = |P|\, K\sqrt{K_c^2 - K^2}, \quad 0 \leqslant K < K_c, \tag{22}$$

maximized at $K_{\mathrm{opt}} = K_c/\sqrt{2}$, where

$$\Gamma_{\max} = \frac{|P|\, K_c^2}{2} = \big|Q_c|\Psi_0|^2 + \tfrac{1}{4}Q_f|\Psi_0|^{1/2}\big|. \tag{23}$$

Equation (22) reduces to the familiar bell-shaped cubic-NLS growth-rate curve when $Q_f = 0$, and is plotted in Fig. 2 for $\kappa = 2$, $b_1 = 1$, and a carrier wave number $k = 2.5$ chosen beyond the zero-nonlinearity point of Fig. 1(b), where $PQ_c > 0$. Figure 2(a) shows the expected increase of both K_c and $\Gamma_{\max}$ with the background amplitude $|\Psi_0|$. Figure 2(b) isolates the effect of the trapped negative-ion population at fixed $|\Psi_0|$: increasing α systematically raises $\Gamma_{\max}$ above the purely Boltzmann ($\alpha \to 0$) value and shifts the optimal wave number K_{opt} slightly upward, showing that trapping does not merely shift the instability threshold but quantitatively enhances the growth of unstable sidebands once instability sets in.

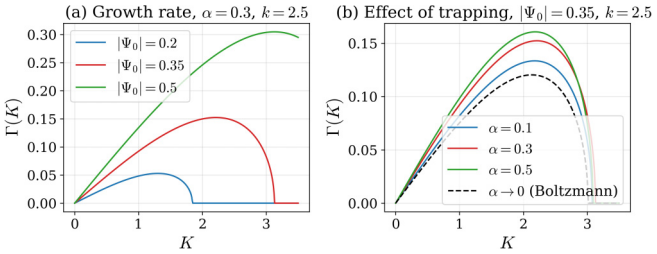


FIG. 2. Modulational instability growth rate $\Gamma(K)$, Eq. (22), for $\kappa = 2$, $b_1 = 1$, $k = 2.5$. (a) Effect of the background amplitude $|\Psi_0|$ at fixed $\alpha = 0.3$. (b) Effect of the negative-ion concentration α at fixed $|\Psi_0| = 0.35$, compared to the purely Boltzmann limit $\alpha \to 0$ (dashed).

B. Optimal negative-ion concentration

Because α enters both D, E, G (through the analytic cascade) and Q_f (linearly, through the trapped-particle term), its effect on the maximum growth rate $\Gamma_{\max}(\alpha)$, Eq. (23), is not monotonic over the full physical range $\alpha \in (0, 1)$ (the limit $\alpha \to 1$ corresponds to a pure positive- or negative-ion plasma with no electrons), as shown in Fig. 3. For $\kappa = 2$, $k = 2.5$, $b_1 = 1$, $|\Psi_0| = 0.35$, $\Gamma_{\max}$ peaks at an interior value $\alpha_{\text{opt}} \simeq 0.555$ ($\Gamma_{\max} \simeq 0.161$), some 34% above the electron-ion limit ($\alpha \to 0$, $\Gamma_{\max} \simeq 0.120$) and 21% above the electron-free limit ($\alpha \to 1$, $\Gamma_{\max} \simeq 0.133$).

This optimum results from the competition between the linear increase of the trapped-particle contribution $Q_f \propto \alpha$ and the nonmonotonic dependence of the cubic coefficient Q_c on α through D, E, G: neither effect dominates uniformly, so their balance peaks at an intermediate concentration rather than at either compositional extreme.

1. Dependence on the temperature ratio: Critical κ

Figure 4 summarizes the modulational-instability landscape in the (α, κ) plane for $k = 2.5$, $b_1 = 1$, and $|\Psi_0| = 0.35$. Figure 4(a) shows the maximum growth rate $\Gamma_{\max}$. The dominant feature is a ridge of optimal growth (red curve), corresponding to the concentration α_{opt} that maximizes $\Gamma_{\max}$ at each κ. For $\kappa < \kappa_c \simeq 1.4$, the optimum remains at the boundary $\alpha = 1$, indicating a monotonic increase in instability with negative-ion concentration. Above κ_c, the optimum moves into the interior of the physical interval $0 < \alpha < 1$, reflecting the competition between the trapped-particle contribution ($Q_f \propto \alpha$) and the α-dependent cubic response through D, E, and G. As κ increases, the ridge shifts toward smaller α while the corresponding maximum growth rate increases. The results show that the strongest instability generally occurs at an intermediate negative-ion concentration rather than at either compositional extreme. Figure 4(b) displays the corresponding critical wave number K_c. Together, the two panels demonstrate that the strongest modulational instability is governed not simply by the width of the unstable band (K_c), but by the interplay between the cubic and trapped-particle nonlinearities, which produces a well-defined optimal concentration once $\kappa > \kappa_c$.

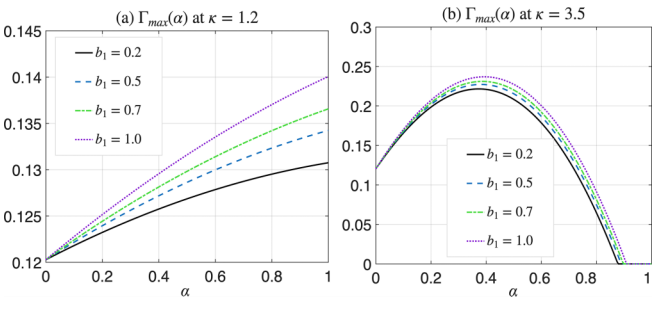


FIG. 3. Dependence of the maximum growth rate $\Gamma_{\max}$ on negative-ion concentration α for several trapping strengths b_1. For $\kappa = 1.2 < \kappa_c$ (a), $\Gamma_{\max}$ increases monotonically and reaches its maximum at $\alpha = 1$. For $\kappa = 3.5 > \kappa_c$ (b), an interior optimum appears near $\alpha \simeq 0.4$, with instability suppression at sufficiently large α. Stronger trapping amplifies the instability but only weakly shifts the optimum concentration.

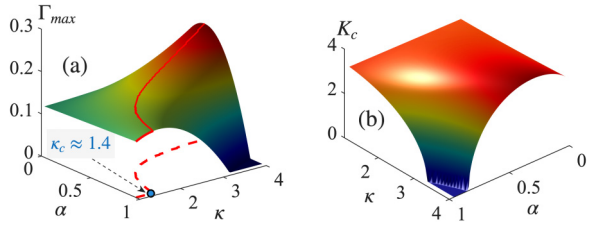


FIG. 4. Contour maps of (a) the maximum modulational-instability growth rate $\Gamma_{\max}$ and (b) the critical instability wave number K_c in the (α, κ) plane for $k = 2.5$, $b_1 = 1$, and $|\Psi_0| = 0.35$. The red curve in panel (a) identifies the locus of optimal negative-ion concentration α_{opt}. A critical temperature ratio $\kappa_c \simeq 1.4$ separates two regimes: for $\kappa < \kappa_c$, the instability increases monotonically with α and is maximized at $\alpha = 1$; for $\kappa > \kappa_c$, an interior optimum emerges and shifts toward lower α as κ increases.

2. Near-threshold behavior

The carrier wave number also interacts nontrivially with α close to the long-wavelength instability threshold of Fig. 1(b) ($k \simeq 1.43$ at $\kappa = 2$). Figure 5 compares $\Gamma_{\max}(\alpha)$ at $k = 1.5$ and $k = 1.75$ (just above threshold) to the reference case

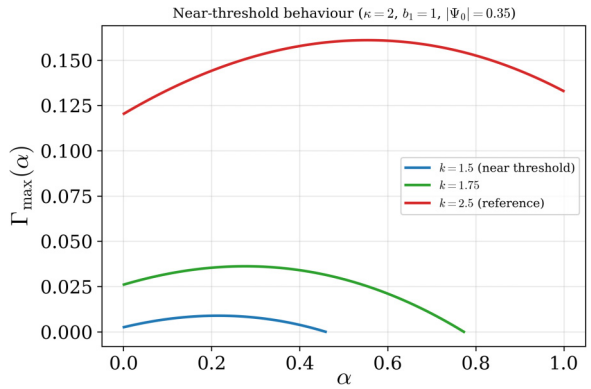


FIG. 5. Maximum growth rate $\Gamma_{\max}(\alpha)$ for carrier wave numbers close to the long-wavelength instability threshold ($k = 1.5, 1.75$) compared to the reference value $k = 2.5$, at $\kappa = 2$, $b_1 = 1$, $|\Psi_0| = 0.35$. Near threshold, sufficiently large α suppresses the instability entirely.

$k = 2.5$. Sufficiently close to threshold, increasing α does not merely change the magnitude of the instability: it can suppress it entirely. At $k = 1.5$, $\Gamma_{\max}(\alpha)$ rises from a small value at $\alpha = 0$, peaks near $\alpha \simeq 0.22$, and falls to zero by $\alpha \simeq 0.46$: beyond this point the system is modulationally stable at every K, regardless of background amplitude. The same qualitative behavior persists, with a wider window, at $k = 1.75$ (extinction near $\alpha \simeq 0.77$), and disappears once k is far enough from threshold [the $k = 2.5$ curve spans the full range $\alpha \in (0, 1)$]. Near threshold, the negative-ion concentration is therefore not just an instability-strength control parameter but can act as an on-off switch for the instability itself, through its effect on the sign of $Q_c(k, \alpha)$ in Eq. (21).

The existence of an interior optimum away from threshold is therefore qualitatively robust above κ_c, but its location is sensitive to the remaining parameters, most strongly to the carrier wave number, as just described, and mildly to the trapping amplitude b_1 (which shifts α_{opt} upward slightly as it increases). The overall conclusion (that an intermediate negative-ion concentration generally maximizes the modulational growth rate, rather than either the electron-dominated or electron-free limit, except sufficiently close to $\kappa = 1$ or to the long-wavelength threshold in k) holds throughout the parameter ranges explored here.

Taken together, Figs. 1–5 cover the full parameter space systematically: the carrier wave number k (Figs. 1 and 5), the negative-ion concentration α (Figs. 2 and 3), the electron-to-negative-ion temperature ratio κ (Fig. 4), and the trapping amplitude b_1 (at the reference value $b_1 = 1$ throughout Figs. 1 to 5, and compared with $b_1 = 5$ in the rogue-wave simulations of Sec. VII). The qualitative conclusions (nonmonotonic $\Gamma_{\max}(\alpha)$ with an interior optimum above $\kappa_c \simeq 1.4$, and a finite instability window that closes near the long-wavelength threshold) are robust across the parameter ranges explored here and are not specific to the representative values used for illustration.

VII. ROGUE WAVE DYNAMICS

The growth rate of Sec. VI A describes the linear onset of MI; its nonlinear outcome is conventionally captured, for the pure cubic NLS, by the Peregrine breather, the simplest rational rogue-wave solution, rising to three times the background amplitude before symmetrically decaying back to it. For the purely Boltzmann (analytic) electronegative plasma, the Peregrine, Akhmediev, and Kuznetsov-Ma solutions, together with their dependence on the negative-ion concentration and temperature ratio, have already been characterized in detail [8,10]; this is the $b_1 \to 0$ limit against which the present results should be compared. No closed-form analog of these solutions is known for the mixed equation (16). However, in the parameter regimes explored above the fractional term is generically a small fraction of the cubic one (e.g., $|Q_f/Q_c| \simeq 0.07$ at the reference point $\kappa = 2$, $k = 2.5$, $\alpha = 0.555$, $b_1 = 1$), so its effect on an otherwise-Peregrine rogue wave can be assessed directly by numerical integration.

A. Rescaling to standard form

The cubic-only truncation of Eq. (16) ($Q_f = 0$) admits the standard rogue-wave family once written in normalized form. For $PQ_c > 0$ (the instability condition of Sec. VI), the substitution $\Psi(\zeta, \sigma) = \Psi_0 \phi(X, T)$, $\zeta = LX$, $\sigma = T_c T$, $T_c = \frac{1}{Q_c \Psi_0^2}$, $L = \frac{\sqrt{2PT_c}}{\Psi_0}$ (with $PT_c > 0$ guaranteed by $PQ_c > 0$, so that L is real) reduces the cubic-only equation exactly to

$$\mathrm{i}\,\partial_T \phi + \tfrac{1}{2}\partial_X^2 \phi + |\phi|^2 \phi = 0, \tag{24}$$

whose rational (Peregrine [2]) and periodic (Akhmediev [3]) breather solutions are well known in closed form

$$\phi_{\text{P}}(X, T) = 1 - \frac{4(1 + 2\mathrm{i}T)}{1 + 4X^2 + 4T^2}, \tag{25}$$

$$\phi_{\text{AB}}(X, T; a) = 1 + \frac{2(1 - 2a)\cosh(bT) + \mathrm{i}b \sinh(bT)}{\sqrt{2a}\cos(pX) - \cosh(bT)}, \tag{26}$$

with $p = 2\sqrt{1 - 2a}$, $b = \sqrt{8a(1 - 2a)}$, for $0 < a < 1/2$; $\phi_{\text{AB}} \to \phi_{\text{P}}$ as $a \to 1/2$. Both rise from the unit background to a peak at $X = T = 0$ [3 for the Peregrine soliton; $1 + 2(1 - 2a)/(\sqrt{2a} - 1)$ for the Akhmediev breather (AB)] and decay symmetrically in T. Neither closed form involves Q_f: both are solutions of the cubic truncation only, and the rescaling (Sec. VII A) itself is built from P and Q_c alone.

We use $\Psi_{\text{rogue}}(\zeta, \sigma) = \Psi_0\, \phi(\zeta/L, \sigma/T_c)$, with $\phi = \phi_{\text{P}}$ or ϕ_{AB}, as the initial condition for the full equation (16) (i.e., including Q_f), which is then integrated directly in the original physical variables (ζ, σ) by split-step Fourier; Q_f enters only here, through the nonlinear propagator $\exp[\mathrm{i}(Q_c|\Psi|^2 + Q_f|\Psi|^{1/2})\, d\sigma]$ applied at each time step, never in a closed-form expression for the field itself. Setting $Q_f = 0$ in the same integrator and comparing against ϕ evaluated through Sec. VII A provides the exact reference curves quoted below. At the reference point $\kappa = 2$, $k = 2.5$, $\alpha = 0.555$ used throughout this section, $T_c = -0.827$, $L = 0.238$.

B. Peregrine soliton: Method and validation

Equation (16) is solved by a symmetric split-step Fourier scheme, initializing the field with the exact Peregrine solution of the background cubic equation ($Q_f = 0$) well before its peak, and propagating forward in physical time σ through the rogue event. The scheme uses $N_\zeta = 4096$ grid points on a periodic spatial domain of length $80L$, with $N_\sigma = 8000$ time steps over a total propagation range of $6.4\,|T_c|$; for the AB the domain length equals exactly one spatial period $2\pi L/p$. Boundary conditions are periodic in ζ throughout. Two independent convergence tests are performed. First, with $Q_f = 0$, the scheme reproduces the exact Peregrine (Akhmediev) peak amplitude to five significant digits. Second, doubling both N_ζ and N_σ leaves all reported amplitudes and deviation ratios unchanged to within 0.1%, confirming that the observed time-asymmetry is a physical effect rather than a numerical artefact.

C. Peregrine soliton: Results

At the reference trapping amplitude $b_1 = 1$, the peak amplitude is essentially unaffected ($2.998\,\Psi_0$ versus the exact $3\,\Psi_0$), but the trapped-ion term breaks the time-symmetry

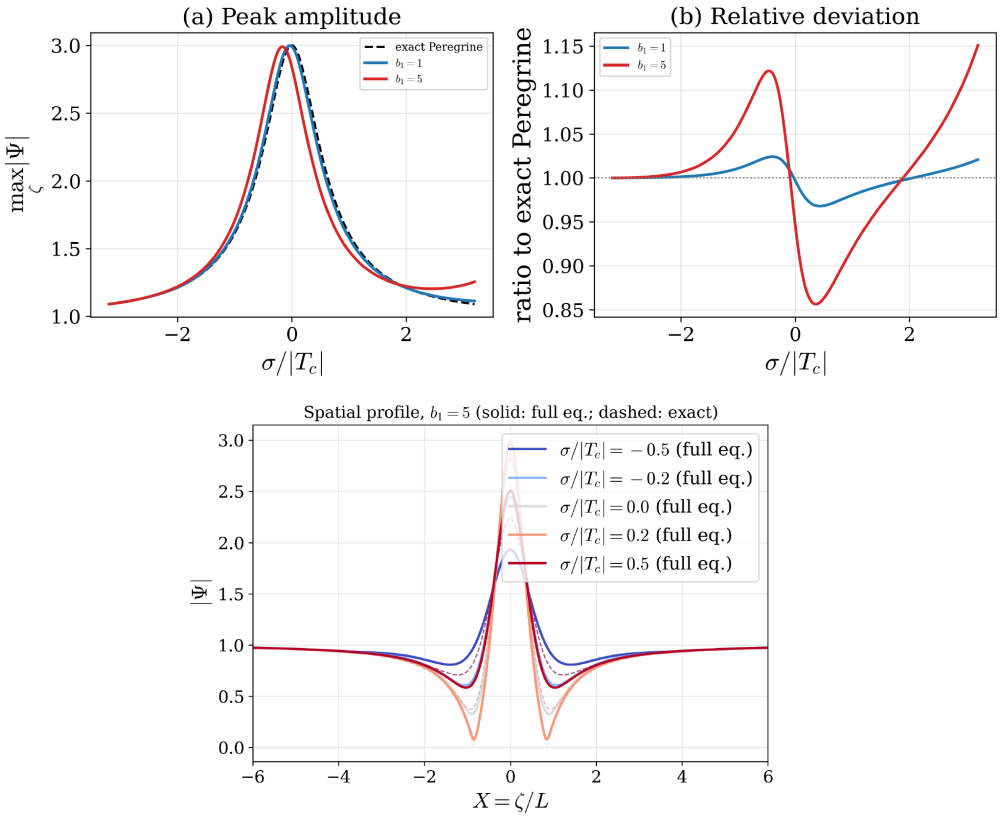


FIG. 6. Top: peak amplitude $\max_\zeta |\Psi|$ versus physical time σ for the full Schamel-NLS equation at $b_1 = 1$ and $b_1 = 5$, compared to the exact Peregrine soliton of the background cubic equation ($Q_f = 0$), at $\kappa = 2$, $k = 2.5$, $\alpha = 0.555$. Bottom: spatial profiles $|\Psi(\zeta)|$ at five values of $\sigma/|T_c|$ for $b_1 = 5$ (solid), compared to the exact Peregrine profile at the same time (dashed).

that is exact for the pure Peregrine soliton: Fig. 6(a) shows an amplification of up to $+2.4\%$ relative to the exact solution before the peak ($\sigma < 0$) and a suppression of up to -3.2% after it ($\sigma > 0$). At a stronger trapping amplitude $b_1 = 5$ ($|Q_f/Q_c| \simeq 0.36$), the same asymmetry is far more pronounced ($+12\%$ before, -14% at its deepest after), and, importantly, the field no longer relaxes back to the background level once the rogue event has passed: Fig. 6(a) shows it settling onto an elevated plateau ($\simeq 1.25\,\Psi_0$ rather than the background $1.09\,\Psi_0$), and the corresponding spatial profiles [Fig. 6(b)] confirm that this is a genuine, well-resolved redistribution of the field rather than a numerical artefact: the prepeak profile ($\sigma/|T_c| = -0.5$) is taller and narrower than the exact Peregrine at the same time, while the postpeak profile ($\sigma/|T_c| = +0.5$) is broader and flatter, with residual energy left in the surrounding pedestal.

D. Akhmediev breather

The Peregrine soliton is the infinite-period limit of the AB; the exact solution describing the nonlinear saturation of a single unstable Fourier mode of the MI spectrum, periodic in ζ and localized in σ. Since Sec. VI A characterizes exactly this linear growth, the AB provides a direct nonlinear continuation of the growth-rate analysis, and we repeat the procedure of Sec. VII A using $\phi_{\rm AB}$, Eq. (26), with $a = 0.25$ (giving $p = \sqrt{2}$ and peak amplitude $\simeq 2.414\,\Psi_0$) as the initial condition, on a spatial domain equal to exactly one breather period $2\pi L/p$. The $Q_f = 0$ check again reproduces the exact peak to five significant digits.

Figure 7 shows that the AB displays the same qualitative time-asymmetry as the Peregrine soliton, somewhat more pronounced at equal trapping strength ($+15\%/-17\%$ at $b_1 = 5$, versus $+12\%/-14\%$ for Peregrine). In addition, and unlike the Peregrine case, the saturation amplitude itself increases systematically with trapping: $2.414\,\Psi_0 \to 2.421\,\Psi_0$ ($b_1 = 1$) $\to 2.445\,\Psi_0$ ($b_1 = 5$). This is expected: the AB is precisely the nonlinear outcome of the same mode whose linear growth rate $\Gamma(K)$ was already shown in Sec. VI A to increase with the trapped-ion population: a larger growth rate plausibly drives the mode to a higher nonlinear saturation level.

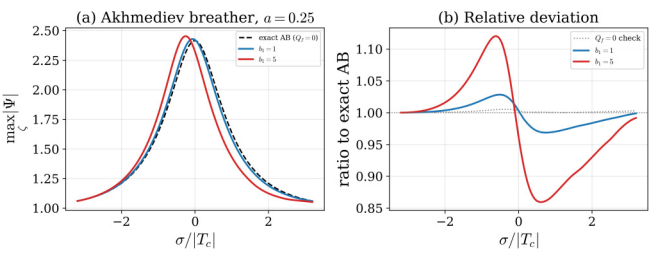


FIG. 7. Peak amplitude $\max_\zeta |\Psi|$ versus physical time σ for the Akhmediev breather ($a = 0.25$) of the full Schamel-NLS equation at $b_1 = 1$ and $b_1 = 5$, compared to the exact breather of the background cubic equation ($Q_f = 0$), at the same parameters as Fig. 6.

E. Interpretation

The trapped-ion population thus introduces a qualitative, testable signature beyond the modulational threshold and growth rate of Secs. VI to VI B: the resulting rogue wave builds up faster than it decays, rather than evolving symmetrically as the classic Peregrine and Akhmediev solutions do, and, at sufficiently strong trapping, leaves the background persistently perturbed (in the Peregrine case) or saturates at a measurably higher amplitude (in the periodic Akhmediev case) rather than reproducing the purely cubic result. Neither feature would be visible from the peak amplitude of the Peregrine soliton alone, which remains close to $3\Psi_0$ throughout. Unlike the peak amplitude, which remains almost unchanged, the temporal asymmetry thus provides a far more sensitive indicator of trapped-particle effects; experiments aiming to detect such effects should accordingly focus on the temporal evolution of the wave around the rogue event rather than on its maximum amplitude alone.

We emphasize that these are perturbative and numerical results rather than closed-form solutions; constructing exact rogue-wave analogues for the mixed cubic-fractional equation (16),for instance via a variational (Lagrangian) ansatz, remains an open problem. The third member of the standard rogue-wave family, the Kuznetsov-Ma soliton [4,5] (localized in ζ, periodic in σ), is not analyzed here; given the consistent pattern found for both the Peregrine and Akhmediev cases, we expect a qualitatively similar time asymmetry, but confirming this is left for future work.

VIII. DISCUSSION

The present derivation highlights an important distinction between analytic equilibrium closures and trapped-particle descriptions. Within the framework considered here, only the latter generate the fractional nonlinear contribution appearing in Eq. (16), so a nonzero Q_f can be read as a signature of a genuinely kinetic, out-of-equilibrium population, namely, particles trapped in the wave's own potential, that no fluid closure based on a thermalized, analytic distribution (Boltzmann, Tsallis, κ, Cairns) captures. Observationally, this connects the present model to the broader, well-documented family of trapped-particle structures, including electron and ion holes, BGK modes [13], and the electrostatic solitary waves recorded *in situ* by spacecraft such as Cluster, FAST, Geotail, and MMS in the auroral zone, the magnetosphere, and the solar wind [14,15], which are conventionally modeled by single-pulse Schamel-type equations. The present derivation provides the corresponding framework for their amplitude modulation, relevant whenever such structures are organized in modulated wave trains rather than isolated pulses.

For the specific system considered here, the regimes in which trapped negative ions (rather than the more commonly studied trapped electrons) are expected to matter include the lower ionosphere, cometary and dusty plasmas, and electronegative processing plasmas. The most actionable outcome of Secs. VI to VI B is that the effect of trapping on modulational stability is not monotonic in the negative-ion fraction α: depending on the temperature ratio κ and the carrier wave number k, there exists either an intermediate α that maximizes the instability growth rate (Sec. VI B), or, sufficiently close to the long-wavelength threshold, a finite window of α outside of which the instability is suppressed entirely (Fig. 5). Neither behavior would be anticipated from the sign of Q_f alone, and both constitute falsifiable, parameter-specific predictions that distinguish this model from the purely Boltzmann case of [7].

Although the fractional contribution remains smaller than the cubic term over a large part of the parameter space explored here (typically $|Q_f/Q_c| \sim 0.05$–0.1 at the reference points used throughout this paper), its qualitative influence is significant because it alters the symmetry of the rogue-wave evolution rather than simply rescaling its amplitude (Sec. VII). This suggests that even a comparatively weak trapped-particle population may leave experimentally observable signatures, through the timing asymmetry of an individual rogue event rather than through its peak amplitude alone.

IX. CONCLUSION

Starting from the electronegative plasma model of [7], our analysis indicates that, within the reductive perturbation framework considered here, analytic equilibrium closures systematically lead to cubic envelope equations, with the closure only reshaping P and Q. Introducing a fractional-order envelope nonlinearity therefore requires a nonanalytic closure, such as the Schamel trapped-particle distribution adopted in the present work, applied here to the negative-ion population rather than to the electrons as in prior electronegative treatments [17]. Both the long-wavelength (Gardner-Schamel) and modulated-wave-packet (Schamel-NLS) limits of the resulting model were derived, the distinguished orderings of the trapping parameter required for a self-consistent balance in each case were identified (these differ between the two limits of the same physical system), and the dispersion, cubic, and fractional coefficients of the Schamel-NLS equation were obtained in closed form. Unlike existing Schamel-NLSE derivations for other physical systems [12,18], the resulting equation retains both the standard cubic and the fractional contributions self-consistently, reducing correctly to the purely cubic result of [7] as $\alpha \to 0$ and to a purely fractional Schamel-NLSE as the analytic cascade is suppressed. The modulational stability criterion, Eq. (21), generalizes the standard cubic-NLS and pure Schamel-NLSE criteria and shows explicitly how the trapped-ion population can shift, and potentially reverse, the stability profile relative to the purely Boltzmann case. Numerically, we further find that the maximum growth rate is nonmonotonic in the negative-ion concentration α: an intermediate value $\alpha_{\mathrm{opt}} \in (0, 1)$, sensitive mainly to the carrier wave number and the temperature ratio κ, maximizes the instability relative to both the electron-dominated and electron-free limits. Beyond this modulational analysis, the rogue-wave simulations of Sec. VII reveal a second, qualitatively distinct signature of trapping: a breaking of the time-symmetry of the Peregrine and Akhmediev solutions, such that the resulting rogue wave builds up faster than it decays even when its peak amplitude is essentially unchanged. Of the results reported here, this nonmonotonic optimal concentration and the temporal asymmetry of the rogue-wave dynamics constitute the clearest and most

directly testable signatures of trapped negative ions in this system.

The methodology developed here is not restricted to electronegative plasmas: because the derivation relies mainly on the trapped-particle closure rather than on any detail of the electronegative composition, similar fractional envelope equations may arise in other plasma configurations, such as magnetized, dusty, or multidimensional plasmas, where kinetic trapping plays a significant role. Exploring such extensions constitutes a promising direction for future work.

DATA AVAILABILITY

There are no publicly available research data or software supporting this manuscript. Requests for further information or data should be sent to the authors.

[1] T. B. Benjamin and J. E. Feir, The disintegration of wave trains on deep water part 1. Theory, J. Fluid Mech. **27**, 417 (1967).

[2] D. H. Peregrine, Water waves, nonlinear Schrödinger equations and their solutions, J. Austral. Math. Soc. Ser. B **25**, 16 (1983).

[3] N. Akhmediev, V. M. Eleonskii, and N. E. Kulagin, Exact first-order solutions of the nonlinear Schrdinger equation, Sov. Phys. JETP **62**, 894 (1985).

[4] E. A. Kuznetsov, Solitons in a parametrically unstable plasma, Sov. Phys. Dokl. **22**, 507 (1977).

[5] Y.-C. Ma, The perturbed plane-wave solutions of the cubic Schrödinger equation, Stud. Appl. Math. **60**, 43 (1979).

[6] S. V. Vladimirov, V. N. Tsytovich, S. I. Popel, and F. K. Khakimov, *Modulational Interactions in Plasmas* (Kluwer Academic, Dordrecht, The Netherlands, 1995).

[7] C. S. Panguetna, C. B. Tabi, and T. C. Kofané, Electronegative nonlinear oscillating modes in plasmas, Commun. Nonlinear Sci. Numer. Simul. **55**, 326 (2018).

[8] C. S. Panguetna, C. B. Tabi, and T. C. Kofané, Low relativistic effects on the modulational instability of rogue waves in electronegative plasmas, J. Theor. Appl. Phys. **13**, 237 (2019).

[9] S. A. El-Tantawy, Rogue waves in electronegative space plasmas: The link between the family of the KdV equations and the nonlinear Schrödinger equation, Astrophys. Space Sci. **361**, 164 (2016).

[10] H. M. Abdelhamid and Z. Yoshida, Nonlinear helicons bearing multi-scale structures, Phys. Plasmas **24**, 022107 (2017).

[11] H. Schamel, Stationary solitary, snoidal and sinusoidal ion acoustic waves, Plasma Phys. **14**, 905 (1972).

[12] H. Demiray, Modulation of electron-acoustic waves in a plasma with vortex electron distribution, Int. J. Nonlin. Sci. Numer. Simul. **16**, 61 (2015).

[13] I. B. Bernstein, J. M. Greene, and M. D. Kruskal, Exact nonlinear plasma oscillations, Phys. Rev. **108**, 546 (1957).

[14] H. Matsumoto, H. Kojima, T. Miyatake, Y. Omura, M. Okada, I. Nagano, and M. Tsutsui, Electrostatic solitary waves (ESW) in the magnetotail: BEN wave forms observed by GEOTAIL, Geophys. Res. Lett. **21**, 2915 (1994).

[15] R. E. Ergun, C. W. Carlson, J. P. McFadden, F. S. Mozer, L. Muschietti, I. Roth, and R. J. Strangeway, Debye-scale plasma structures associated with magnetic-field-aligned electric fields, Phys. Rev. Lett. **81**, 826 (1998).

[16] H. Bailung, S. K. Sharma, and Y. Nakamura, Observation of Peregrine solitons in a multicomponent plasma with negative ions, Phys. Rev. Lett. **107**, 255005 (2011).

[17] U. N. Ghosh, Interaction of Schamel type solitary waves in an electronegative plasma with trapped non-extensive electrons, Indian J. Phys. **96**, 2175 (2022).

[18] S. A. El-Tantawy, M. Abu Hammad, B. M. Alotaibi, E. Tag-Eldin, S. M. E. Ismaeel, and E. I. El-Awady, On the modulational of Schamel nonlinear Schrödinger equation and the associated envelope excitations in a degenerate relativistic quantum complex plasma, Results Phys. **51**, 106702 (2023).

[19] L. Djebarni, K. Annou, D. Bennaceur-Doumaz, and Z. Bellahsene, Modeling the modulational instability of ion-acoustic waves in electron-ion plasma with Vasyliunas-Schamel distributed electrons, J. Electromagn. Waves Appl. **39**, 2057 (2025).

[20] F. Wahed, A.-u. Rahman, H. A. Alyousef, L. S. El-Sherif, and S. A. El-Tantawy, Modulational instability and associated low-frequency dust-acoustic waves in a degenerate Thomas-Fermi plasma: Envelope solitons and rogue waves, J. Low Freq. Noise Vib. Act. Control **44**, 784 (2025).

[21] W.-P. Zhang *et al.*, Theoretical study of nonlinear magnetosonic waves: Potential applications in plasma diagnostics, Front. Phys. **20**, 045201 (2025).

[22] S. I. Popel and M. Y. Yu, Modulational interaction of short-wavelength ion-acoustic oscillations in impurity-containing plasmas, Phys. Rev. E **50**, 3060 (1994).

[23] R. Bala and T. S. Gill, Multimode excitation and modulational instability of beam plasma system with Tsallis-distributed electrons, Pramana **95**, 59 (2021).

[24] C. S. Gardner and G. K. Morikawa, Similarity in the asymptotic behavior of collision-free hydromagnetic waves, Tech. Rep. (Courant Institute, New York University, 1960).

[25] I. Kourakis and P. K. Shukla, Modulated dust-acoustic wave packets in a plasma with non-isothermal electrons and ions, J. Plasma Phys. **71**, 185 (2005).

[26] S. I. Popel, V. N. Tsytovich, and S. V. Vladimirov, Modulational instability of Langmuir wave packets, Phys. Plasmas **1**, 2176 (1994).